DOI: 10.1002/chem.200700087

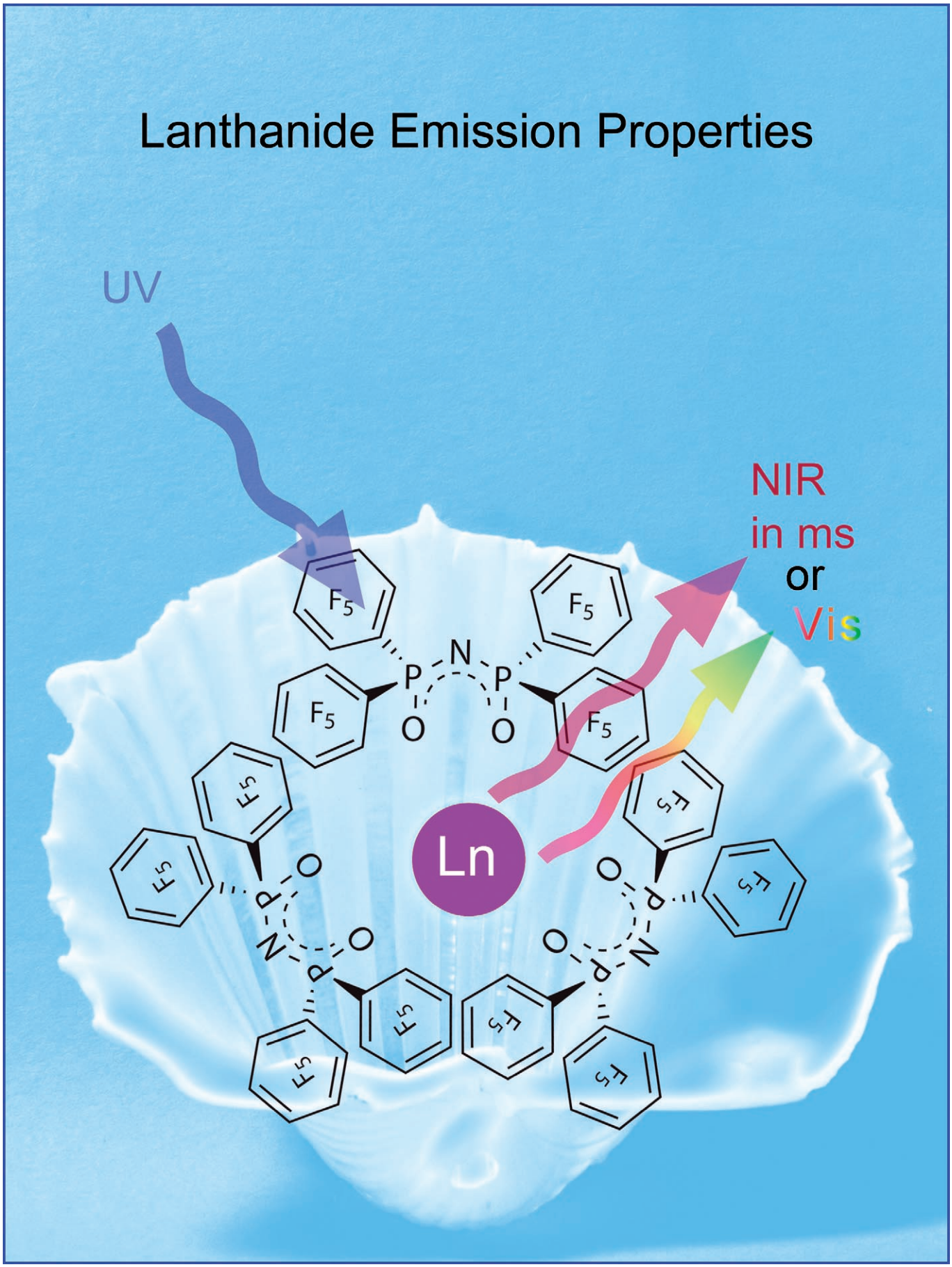

Fully Fluorinated Imidodiphosphinate Shells for Visible- and NIR-Emitting Lanthanides: Hitherto Unexpected Effects of Sensitizer Fluorination on Lanthanide Emission Properties

Peter B. Glover,[a] Andrew P. Bassett,[a] Peter Nockemann,[b] Benson M. Kariuki,[a] Rik Van Deun,[b] and Zoe Pikramenou*[a]

Abstract: In this paper we demonstrate that the effect of aromatic C–F substitution in ligands does not always abide by conventional wisdom for ligand design to enhance sensitisation for visible lanthanide emission, in contrast with NIR emission for which the same effect coupled with shell formation leads to unprecedented long luminescence lifetimes. We have chosen an imidodiphosphinate ligand, *N*-{*P*,*P*-di-(pentafluorophinoyl)}-*P*,*P*-dipentafluorophenylphosphinimidic acid (HF_{20}tpip), to form ideal fluorinated shells about all visible- and NIR-emitting lanthanides. The shell, formed by three ligands, comprises twelve fully fluorinated aryl sensitiser groups, yet no-high energy X–H vibrations that quench lanthanide emission. The synthesis, full characterisation including X-ray and NMR analysis as well as the photophysical properties of the emissive complexes $[Ln(F_{20}tpip)_3]$, in which Ln = Nd, Sm, Eu, Gd, Tb, Dy, Er, Yb, Y, Gd, are reported. The photophysical results contrast previous studies, in which fluorination of alkyl chains tends to lead to more emissive lanthanide complexes for both visible and NIR emission. Analysis of the fluorescence properties of the HF_{20}tpip and $[Gd(F_{20}tpip)_3]$ reveals that there is a low-lying state at around 715 nm that is responsible for partially quenching of the signal of the visible emitting lanthanides and we attribute it to a π–σ^* state. However, all visible emitting lanthanides have long lifetimes and unexpectedly the $[Dy(F_{20}tpip)_3]$ complex shows a lifetime of 0.3 ms, indicating that the elimination of high-energy vibrations from the ligand framework is particularly favourable for Dy. The NIR emitting lanthanides show strong emission signals in powder and solution with unprecedented lifetimes. The luminescence lifetimes of $[Nd(F_{20}tpip)_3]$, $[Er(F_{20}tpip)_3]$ and $[Yb(F_{20}tpip)_3]$ in deuteurated acetonitrile are 44, 741 and 1111 μs. The highest value observed for the $[Yb(F_{20}tpip)_3]$ complex is more than half the value of the Yb ion radiative lifetime.

Keywords: lanthanides · ligand design · luminescence · photochemistry · supramolecular chemistry

Introduction

Self-assembly of ligands around lanthanide ions is a powerful strategy to obtain architectures in which the steric and electronic properties of the ligands control the lanthanide coordination environment. Lanthanide helices,[1–5] wheels,[6–8] starbust shapes,[9] hairpins,[10] racks,[11,12] rotaxanes,[13] squares[14] and other high-dimensional architectures[15–21] have been prepared. When luminescent lanthanides are introduced into these architectures, new properties can be explored for materials and sensing applications.[10,22–27] Optimising ligand design to target efficient sensitisation along with long lanthanide emission lifetimes is of particular interest in the design of lanthanide probes in luminescence imaging of cells.[28] We have been interested in the assembly of shells around the metal using imidodiphosphinates as bind-

[a] P. B. Glover, A. P. Bassett, Dr. B. M. Kariuki, Dr. Z. Pikramenou
School of Chemistry, The University of Birmingham
Edgbaston B15 2TT (UK)
Fax: (+44) 121-414-4446
E-mail: z.pikramenou@bham.ac.uk

[b] Dr. P. Nockemann, Dr. R. V. Deun
Katholieke Universiteit Leuven
Department of Chemistry, Celestijnenlaan 200F
3001 Leuven (Belgium)

Supporting information for this article is available on the WWW under http://www.chemeurj.org/ or from the author. It contains NMR spectra of ligand and complexes, additional UV/Vis, emission and luminescence spectra are available.

ing sites that allow a choice of "remote" sensitiser units.[29–31] A key strategy to achieve long luminescence lifetimes in lanthanide complexes is to eliminate X–H groups with high-energy vibrations from the ligand design. Luminescence is also quenched when solvent molecules containing X–H groups (e.g. water and most common organic solvents) are directly coordinated to the lanthanide. Thus the "ideal" ligand design (not yet achieved) for long lifetimes should be a ligand with no X–H bonds and which excludes solvent coordination to the lanthanide. To try to achieve such an ideal design, we chose to use a fully fluorinated imidodiphosphinate ligand, *N*-(*P*,*P*-dipentafluorophinoyl)-*P*,*P*-dipentafluorophenyl-phosphinimidic acid (HF_{20}tpip). This ligand provides an ideal framework placing twelve "remote" aryl sensitisers about the lanthanide forming a shell and having no CH, NH or OH oscillators in the ligand structure. Although, elimination of high-energy vibrations has been adapted previously in ligand design, the combination of sensitiser units with aromatic C–F substitution and the ability of ligands to form shells around the metal has not been previously reported, hitherto the unexpected luminescence behaviour. Approaches to eliminate high-energy vibrations in ligand structures have shown to be effective for improving sensitisation properties in NIR and visible emission, although the ligands either leave the metal coordinatively unsaturated or do not carry sensitiser units. Approaches involved alkyl chain C–F substitution of diketonate ligands,[32–38] deuteration of podand structures[39] and sulfonylaminate binding sites[40,41] with no sensitiser unit. Our studies not only demonstrate the importance of the fluorinated shell structure around the lanthanide formed by the assembly of three ligands for all the emitting lanthanides, but also provide an understanding of the effect of aromatic C–F substitution in the ligand structure on the photophysical properties of all emitting lanthanides. Indeed, we demonstrate that aromatic fluorination is not suited for sensitisation properties of the visible emitting lanthanides, which is in contrast with the effect of fluorinated alkyl chains in diketonate complexes. During the course of our work,[42] a communication reported the Er complex of the fluorinated tpip ligand albeit with a dual lifetime that would be unexpected in a pure single molecular species[43] and a shorter lifetime to that determined herein.

We have prepared and studied the photophysical properties of the visible and near infra-red emitting complexes of Eu^{III}, Tb^{III}, Sm^{III}, Dy^{III}, Nd^{III}, Er^{III}, Yb^{III}, Y^{III} and Gd^{III}. The analysis of their photophysical properties, allows the evaluation of ligand design for optimum sensitiser function based on the aromatic fluorine substituents.

Results and Discussion

Preparation and characterisation of HF_{20}tpip and [Ln(F_{20}tpip)$_3$] (Ln = Nd, Sm, Eu, Gd, Tb, Dy, Er, Yb, Y, Gd): *N*-(*P*,*P*-dipentafluorophinoyl)-*P*,*P*-dipentafluorophenyl-phosphinimidic acid (HF_{20}tpip) was prepared in two steps (Scheme 1). Bromodipentafluorophenylphosphane was isolated by using a modified procedure[44–46] and then reacted with hexamethyldisilazane and hydrogen peroxide to afford the pure HF_{20}tpip. HF_{20}tpip has been fully characterised by spectroscopic techniques and single-crystal X-ray diffraction.

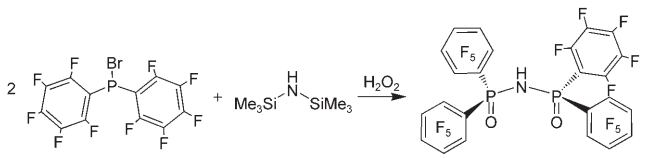

Scheme 1.

The crystal structure of the ligand indicates that the enol-type form of the ligand is present and also contains hexane solvent molecules. Both the P=O bond lengths are equal at 1.503 Å and the angle between them (that is, O1=P1···P2=O2) is 43.81°, and the P–N bond lengths are almost identical at 1.553 and 1.555 Å. This short bond length is indicative of a degree of electron delocalisation around the binding unit, and is consistent to those found for other imidodiphosphinate type ligands.[30] The proton is disordered between the two oxygen atoms and hydrogen bonding occurs between pairs of ligand molecules related by inversion, with an O1···O1′ distance of 2.43 Å (Figure 1 left). The two molecules also interact through π–π contact between rings separated by approximately 3–4 Å, although they are not parallel; the dihedral angle being 14.76°. These pairs interact with neighbouring molecules through edge–face and edge–edge (F–F) contacts to form cages that are occupied by the hexane solvent (Figure 1 right).

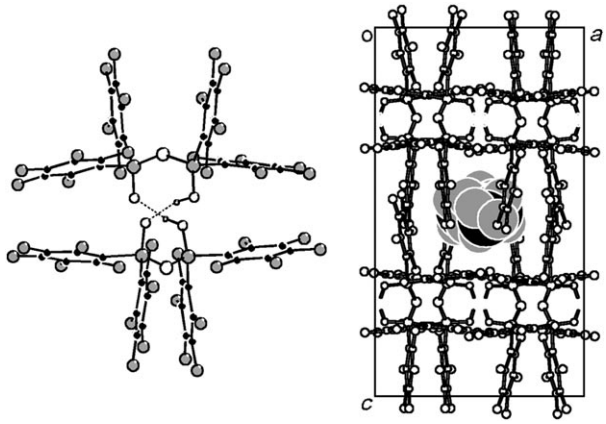

Figure 1. Left: A pair of molecules in the crystal structure of HF_{20}tpip showing hydrogen bonding between two molecules. Right: a segment of the crystal structure viewed down the *b* axis.

The ^{31}P NMR spectrum of HF_{20}tpip shows one phosphorus environment with a resonance at $\delta = -9.0$ ppm. The chemical shift of the resonance is comparable with literature values of fluorinated triarylphosphanes[47,48] and it appears

at a lower frequency in comparison to Htpip, indicating that the phosphorus is more shielded by the presence of the perfluorinated aromatic groups. The ^{19}F NMR spectrum of HF_{20}tpip has three resonances corresponding to the three unique fluorine environments in the ligand, with a ratio of 2:1:2 (Supporting Information) with characteristic ^{3}J(F,F) couplings of 20 Hz. In the ^{13}C NMR spectrum three doublets for the three C–F environments appear with the characteristic 250 Hz ^{1}J(C,F) coupling, while a doublet triplet is assigned to the carbon atom directly bonded to the phosphorus atoms with a 140 Hz ^{1}J(P,C) coupling and two ^{2}J(C,F) couplings of 18 Hz. The absorption spectrum of HF_{20}tpip in ethanol shows an absorbance band at $\lambda_{max}=268$ nm ($\varepsilon=3800\ mol^{-1}\,dm^{3}\,cm^{-1}$).

The lanthanide complexes of HF_{20}tpip were prepared

Table 1. Refinement and crystallographic data for complexes **1**–**7**.

	1	**2**	**3a**	**3b**
formula	$C_{73}H_4F_{60}N_3NdO_7P_6$	$C_{73}H_4F_{60}N_3O_7P_6Sm$	$C_{73}H_4EuF_{60}N_3\ O_7P_6$	$C_{74}H_6EuF_{60}N_3O_7P_6$
T [K]	296	296	293	296
system	triclinic	trigonal	triclinic	triclinic
space group	$P\bar{1}$	$R\bar{3}$	$P\bar{1}$	$P\bar{1}$
a [Å]	14.6917(8)	25.5464(6)	14.6815(12)	14.6612(2)
b [Å]	15.2185(8)	25.5464(6)	15.2316(12)	15.2824(2)
c [Å]	20.6561(10)	22.3700(6)	20.6436(18)	20.6461(3)
α [°]	88.497(4)	90.0	88.104(6)	87.993(1)
β [°]	90.112(4)	90.0	89.913(5)	89.819(1)
γ [°]	64.491(4)	120.0	64.220(5)	64.605(1)
Z	2	6	2	2
V [Å^3]	4166.3(4)	12643.2(5)	4154.2(6)	4176.0(1)
ρ_{calcd} [g cm^{-3}]	1.997	1.961	2.009	2.009
R_1	0.053	0.063	0.057	0.113
wR_2	0.137	0.151	0.139	0.305

	4	**5**	**6**	**7**
formula	$C_{72}F_{60}GdN_3O_6P_6$	$C_{72}DyF_{60}N_3O_6P_6$	$C_{72}ErF_{60}N_3O_6P_6$	$C_{72}F_{60}N_3O_6P_6Yb$
T [K]	298	296	296	296
system	monoclinic	monoclinic	monoclinic	triclinic
space group	$P2/n$	$P2/n$	$P2/n$	$P\bar{1}$
a [Å]	12.3581(3)	12.4095(11)	12.4381(2)	16.152(5)
b [Å]	14.1063(2)	14.0521(10)	13.9971(2)	16.149(5)
c [Å]	23.7628(4)	23.6822(16)	23.6157(4)	23.216(8)
α [°]	90.0	90.0	90.0	86.262(10)
β [°]	90.645(1)	89.388(5)	90.679(1)	70.495(11)
γ [°]	90.0	90.0	90.0	60.111(9)
Z	2	2	2	2
V [Å^3]	4142.2(2)	4129.5(5)	4111.1(1)	4911(3)
ρ_{calcd} [g cm^{-3}]	1.993	2.003	2.016	1.692
R_1	0.036	0.035	0.029	0.14
wR_2	0.092	0.093	0.076	0.31

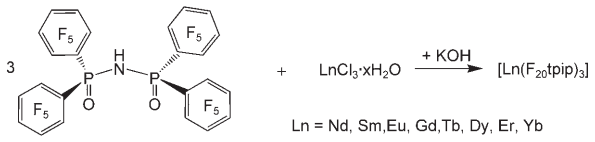

Scheme 2.

(Scheme 2) by addition the desired lanthanide chloride into a solution of the ligand in hot alcohol in a 1:3 ratio either in the presence or absence of a base. We found that, unlike the Htpip reactions, the presence of base did not make any difference in isolation of the complexes, due to the acidic nature of the proton in HF_{20}tpip.

The crystallographic data for the complexes (**1**–**7**) are shown in Table 1. The seven complexes fall into four types of structures as described below.

1) In the structures of the Nd (**1**), and Eu (**3a** and **3b**), the cation coordination and crystal packing are similar. This is reflected by the similar unit cell parameters (Table 1) and the three complexes are shown in Figure 2a–c. Thus, the details of just one will be described. In the structure of **1**, the Nd is coordinated by a methanol molecule in addition to the three F_{20}tpip ligands (Figure 2a). Close π–π contact occurs within a single complex unit between rings separated by a distance of approximately 3–4 Å, although they are not parallel (the dihedral angle is about 20.18°). The arrangement of ligands leaves a gap on one side of the complex, which accommodates a molecule of methanol that is coordinated to the lanthanide cation (Figure 2d). The contacts between neighbouring complex units are mainly between the fluorine atoms, with some slightly less than the combined van der Waals radii. For **1**, the Nd–O distances are in the range 2.375(4)–2.432(4) Å for the ligand and 2.469(5) for methanol. One O=P···P=O torsion angle (1.40(1)°) is less than the other two (9.59(1), 8.95(1)°). For **3a** and **3b**, the Eu–O distances are in the range 2.330(4)–2.391(4) Å and 2.327(7)–2.403(6) Å for the ligand and 2.433(5) and 2.398(10) for the coordinated solvent, respectively.
2) The structure of Sm (**2**) complex consists of the molecular unit co-crystallised with methanol. The complex unit has threefold symmetry and the oxygen atoms coordinate to the cation in propeller-like or distorted trigonal antiprism geometry (Figure 3 top) with an Sm–O distance of 2.329(4) Å. For the ligand, the O=P···P=O torsion angle is −1.96(1)°. Within the cluster unit, all $-C_6F_5$ units are involved in edge–face interactions as either donor or acceptor. The occluded solvent does not coordinate to the cation, but is contained in cylindrical cages formed by

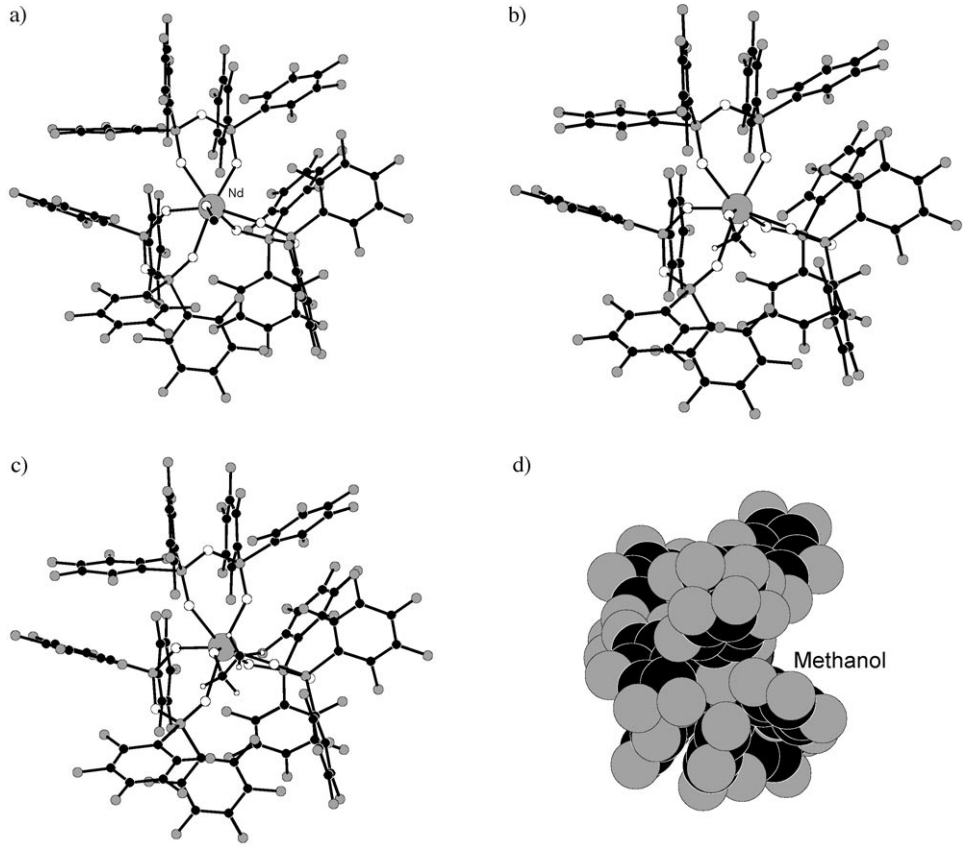

Figure 2. The complexes of a) **1**, b) **3a**, c) **3b** and d) a space filling representation of **1** with the methanol molecule omitted to show the slot it occupies

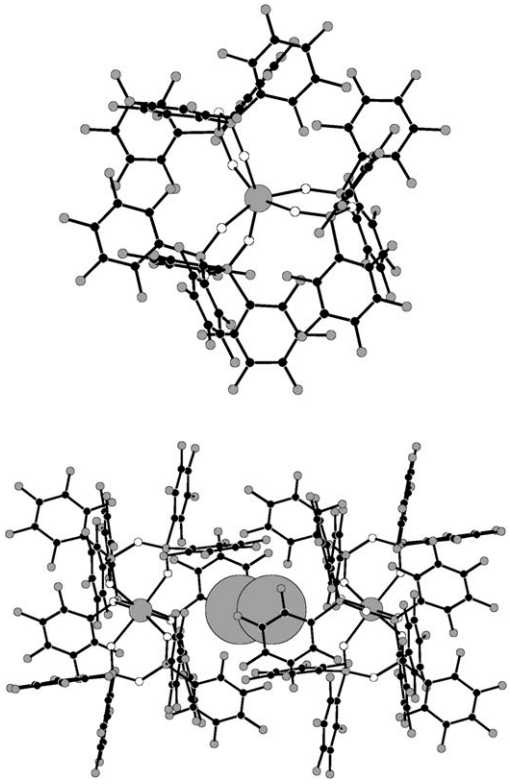

Figure 3. Top: The molecular unit of **2**. Bottom: a pair of units enclosing a solvent position.

two molecular units linked by edge-to-face interactions along the *c* axis.

3) In the crystal, the complex units for Gd (**4**), Dy (**5**) and Er (**6**) cations have twofold symmetry and are not solvated Figure 4a–c. The three complexes are isostructural with similar unit cell parameters and symmetry (Table 1). For the ligand, the O=P···P=O angles are about −0.4 and −12° within the cluster and the coordination around the metal is propeller shaped with bonds in the range 2.286(2)–2.290(2) Å for Gd, 2.258(2)–2.263(2) Å for Dy and 2.2315(16)–2.241(15) Å for Er. The molecular units interact with neighbours mainly through F···F contacts, edge-to-face interactions and interactions of π–π type also occur (Figure 4d).
4) In the structure obtained for **7**, the Yb ion is not coordinated by solvent and has a distorted octahedral geometry (Figure 5 top) with Yb–O distances in the range 2.18(2)–2.28(2) Å. For the ligand, the O=P···P=O torsion angles are −0.3.37(3), −3.35(3) and −4.29(3)°. In a manner similar to the structure of **2**, complex units interact through edge-to-face contacts to form stacks along the *c* axis (Figure 5 bottom). Cylindrical cages are also formed in this structure, but no solvent was found in this case. However, the calculated density is very low when compared to the structures of other complexes. This, combined with the fact that the quality of data was low, suggests that there is likely to be solvent, most likely disordered, in the cages.

A detailed ^{19}F and ^{31}P NMR study of the $[Ln(F_{20}tpip)_3]$ complexes (Ln = Y, Nd, Sm, Eu, Tb, Dy, Er, Yb) has been carried out. A summary of the NMR data of the complexes is given in Table 2.

The phosphorus atoms are the closest to the lanthanide ion and consequently offer much useful information on the properties of the $[Ln(F_{20}tpip)_3]$ complexes. Upon coordination of $F_{20}tpip$ to Y^{III}, the ^{31}P resonance of the ligand moves downfield from $\delta = -9$ to -3 ppm, indicative of the deshielding effect of the phosphorus atoms upon coordination to the lanthanide ion. The ^{31}P NMR spectra of the $[Ln(F_{20}tpip)_3]$ complexes display a single resonance, indicating

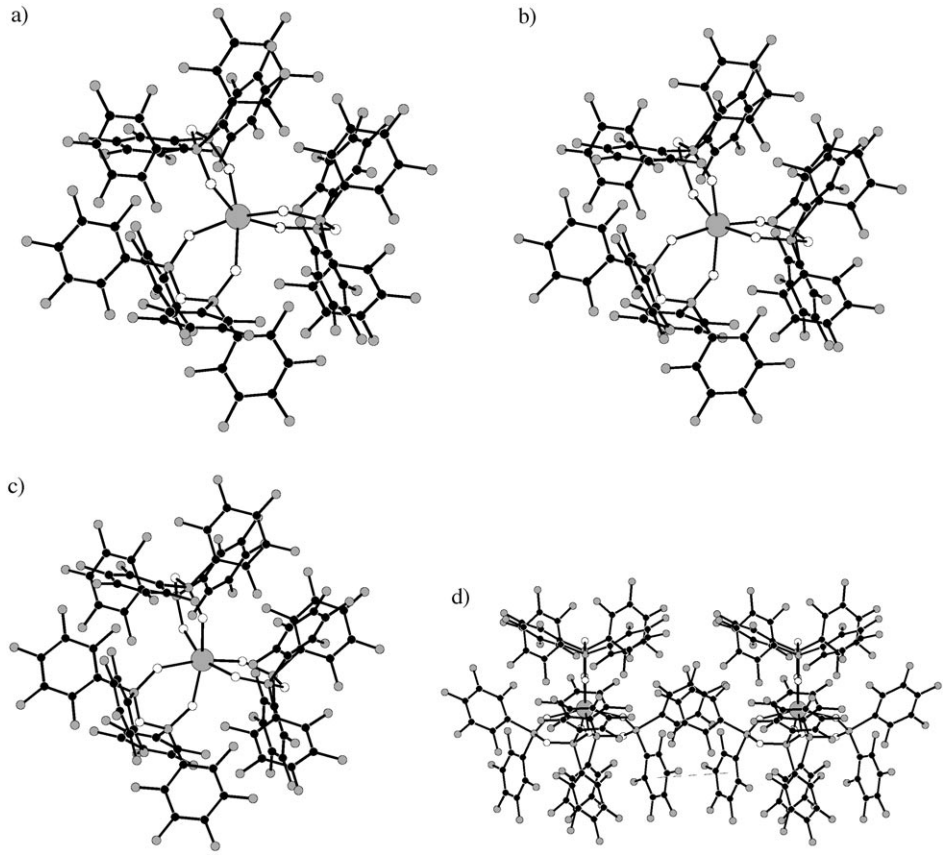

Figure 4. Complexes a) **4**, b) **5**, c) **6** and d) a pair of molecules with a π–π interaction for a pair of rings showing overlap of 1/3 of a ring.

the presence one phosphorus environment for the six phosphorus atoms of the complexes and confirm the equivalence of the ligands. The ^{31}P chemical shifts of $[Ln(F_{20}tpip)_3]$ divide into three groups with respect to the $[Y(F_{20}tpip)_3]$ diamagnetic analogue. The Er^{III} and Eu^{III} complexes display the greatest up field ^{31}P shifts, while the Nd^{III} complex has the largest downfield shift. In the previous report,[43] surprisingly no shift was observed between the ligand signal and the $[Er(F_{20}tpip)_3]$. The shifts of the Sm^{III}, Tb^{III}, Dy^{III} and Yb^{III} complexes remain similar to that of the Y^{III} complex. This can be explained by the paramagnetic shift being a combination of the pseudocontact and contact shifts.[49,50] In the NMR spectra of complexes of paramagnetic metal ions, there are two main additive contributing interactions to the chemical shifts of the ligand nuclei with the paramagnetic nucleus: contact and pseudocontact. The contact shift for a nucleus is determined by covalent bonding interactions transferring unpaired electron density onto the ligand. This effect is most pronounced with ligand nuclei that are very close to the metal ion. The pseudocontact shift arises from through space interaction of the unpaired electron and the nuclear magnetic dipole.[49]

The ^{19}F spectra of the $[Ln(F_{20}tpip)_3]$ complexes are very similar to each other, with the three resonances in a 2:1:2 ratio at similar chemical shifts (Supporting Information). The presence of three sets of resonances for the twenty fluorine atoms of each complex indicates that all of the aromatic rings are equivalent in solution. In the Nd^{III}, Sm^{III}, Eu^{III} and Y^{III} complexes the resonances are sharp revealing $^3J(F,F)$ couplings in the order of 20 Hz, consistent with fluorine atoms in aromatic compounds. The ^{19}F resonances observed in the analogous Tb^{III}, Dy^{III}, Er^{III} and Yb^{III} complexes are broad, obscuring their multiplicity, which is an effect of the different lanthanide paramagnetism.

The ^{13}C NMR spectrum of $[Sm(F_{20}tpip)_3]$ in $[D_6]$acetone allows complete assignments with all the expected information (Supporting Information). Four distinct resonances are observed that correspond to the four unique carbon environments in the complex. The $^1J(C,F)$ coupling of approximately 250 Hz splits the signals of the three C–F carbons into three doublets. The signal for the carbon atom directly bonded to the phosphorus atom splits with a 144 Hz $^1J(P,C)$ coupling and two $^2J(C,F)$ couplings of 18 Hz to give a doublet–triplet pattern. In the rest of the ^{13}C NMR spectra of the $[Ln(F_{20}tpip)_3]$ complexes, limited solubility hampered the observation of some signals, in particular those of the quaternary carbons.

Steady-state luminescence studies of $[Ln(F_{20}tpip)_3]$ in the visible and NIR regions, in which Ln = Eu, Tb, Sm, Dy, Nd, Er, Yb: Upon excitation of the ligand absorption band at 270 nm, characteristic narrow band red, green, pink and yellow emission is observed for the Eu^{III}, Tb^{III}, Sm^{III} and Dy^{III} complexes, respectively (Figure 6). The emission profiles of $[Ln(F_{20}tpip)_3]$ in acetonitrile closely resemble those of the analogous tpip and Metpip complexes,[30] indicating a similar coordination environment in solution. The emission spectra of powder samples of the Tb^{III} and Dy^{III} complexes also show intense emission with similar profiles, indicating no major changes in the coordination environment of the complexes between the solid state and solution. In the case of the Eu^{III} complex, a study of the single crystal allowed observation of a further splitting on the $^5D_0 \rightarrow {}^7F_2$ hypersensitive band, giving three bands centred at 609, 613 and 619 nm. The splitting of the band is a result of the low-symmetry environment around the metal ion (Figure 7). However, in all the solutions of the visible-emitting lanthanides, we

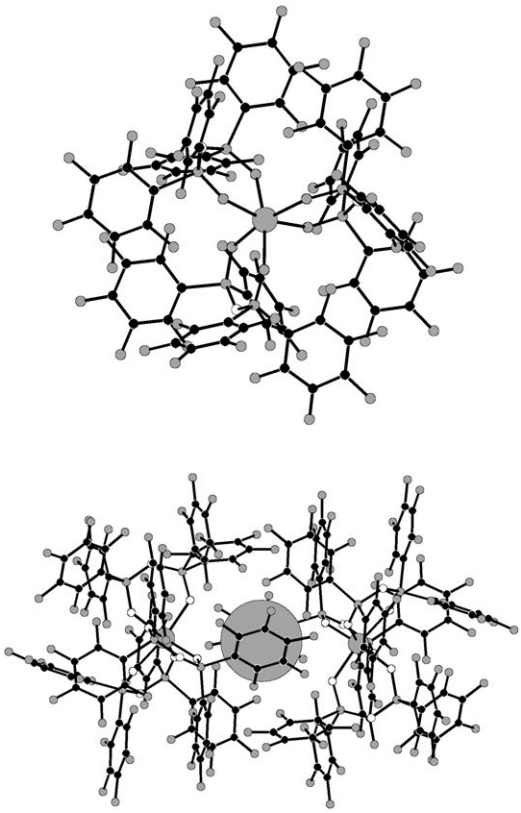

Figure 5. Top: complex **7**. Bottom: a pair of molecules with the cage position highlighted.

Table 2. NMR data for $[Ln(F_{20}tpip)_3]$ in $[D_6]$acetone.

	δ (^{19}F)	δ (^{31}P)
$[Y(F_{20}tpip)_3]$	−133.6 (d, ^3J(F,F) = 20 Hz, 8F; *o*-Ar CF)	−3.2
	−148.3 (t, ^3J(F,F) = 19 Hz, 4F; *p*-Ar CF)	
	−162.1 (dd, ^3J(F,F) = 20 Hz, 8F; *m*-Ar CF)	
$[Nd(F_{20}tpip)_3]$	−133.7 (d, ^3J(F,F) = 19 Hz, 8F; *p*-Ar CF)	7.4
	−149.0 (t, ^3J(F,F) = 20 Hz, 4F; *p*-Ar CF)	
	−162.3 (m, 8F; *m*-Ar CF)	
$[Sm(F_{20}tpip)_3]$	−133.5 (d, ^3J(F,F) = 19 Hz, 8F; *p*-Ar CF)	−3.7
	−148.8 (t, ^3J(F,F) = 20 Hz, 4F; *p*-Ar CF)	
	−162.2 (m, 8F; *m*-Ar CF)	
$[Eu(F_{20}tpip)_3]$	−132.9 (d, ^3J(F,F) = 20 Hz, 8F; *o*-Ar CF)	−39.4
	−148.8 (t, ^3J(F,F) = 20 Hz, 4F; *p*-Ar CF)	
	−162.2 (m, 8F; *m*-Ar CF)	
$[Tb(F_{20}tpip)_3]$	−131.8 (br, 8F; *o*-Ar CF)	−11.5
	−149.2 (br, 4F; *p*-Ar CF)	
	−162.9 (br, 8F; *m*-Ar CF)	
$[Dy(F_{20}tpip)_3]$	−129.7 (br, 8F; *o*-Ar CF)	−3.1
	−149.0 (br, 4F; *p*-Ar CF)	
	−162.5 (br, 8F; *m*-Ar CF)	
$[Er(F_{20}tpip)_3]$	−133.0 (br, 8F; *o*-Ar CF)	−46.6
	−148.0 (br, 4F; *p*-Ar CF)	
	−161.9 (br, 8F; *m*-Ar CF)	
$[Yb(F_{20}tpip)_3]$	−134.6 (br, 8F; *o*-Ar CF)	−0.26
	−147.5 (br, 4F; *p*-Ar CF)	
	−161.9 (br, 8F; *m*-Ar CF)	

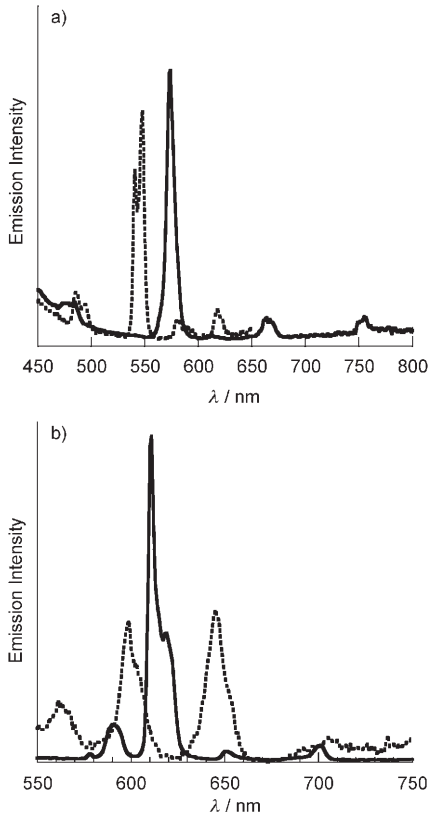

Figure 6. The corrected emission spectra of the visible emitting complexes in acetontitrile, $\lambda_{exc} = 270$ nm. Top: $[Tb(F_{20}tpip)_3]$ (-----) and $[Dy(F_{20}tpip)_3]$ (——) displaying Tb^{III}-based $^5D_4 \rightarrow {}^7F_J$ ($J = 3, 4, 5, 6$) and Dy^{III}-based $^4F_{9/2} \rightarrow {}^6H_J$ ($J = 15/2, 13/2, 11/2, 9/2$) transitions respectively. Bottom: $[Sm(F_{20}tpip)_3]$ (-----) and $[Eu(F_{20}tpip)_3]$ (——) in acetonitrile, displaying Sm^{III}-based $^4G_{5/2} \rightarrow {}^6H_J$, ($J = 5/2$, 7/2, 9/2 and 11/2) and Eu^{III}-based $^5D_0 \rightarrow {}^7F_J$ ($J = 0, 1, 2, 3, 4$) transitions, respectively.

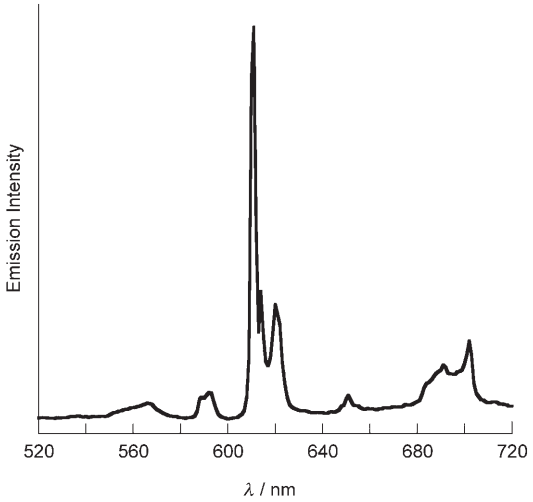

Figure 7. Single crystal luminescence of $[Eu(F_{20}tpip)_3]$, corrected for PMT response, $\lambda_{exc} = 270$ nm.

also observed a background fluorescence band at λ_{max} around 390 nm (Supporting Information). At the first instance we attributed the band to ligand fluorescence (the band is also present in the free ligand) as a result of incomplete energy transfer from the ligand to the lanthanide ion. To confirm that the signal at 390 nm was due to the bound

ligand and not free dissociated ligand, we examined the emission of [Eu(F_{20}tpip)$_3$] upon addition of H_2O and D_2O. Were the F_{20}tpip ligand to be bound to the lanthanide more weakly than the tpip one (due to the withdrawing properties of the twenty fluorine atoms) addition of water would influence the ligand dissociation process. Upon addition of H_2O there is decrease in the lanthanide signal; however, this decrease does not take place upon addition of D_2O (Supporting Information). The relevant intensity ratio of the bands remains constant. These results established the stability of the complexes in the presence of water and further analysis of the H_2O/D_2O effect is performed by time-resolved luminescence studies.

The photophysical properties of [Nd(F_{20}tpip)$_3$], [Er(F_{20}tpip)$_3$] and [Yb(F_{20}tpip)$_3$] in CH_3CN and CD_3CN, as well as in the solid state, have been explored. No ligand fluorescence could be observed at 700 nm. Excitation in the ligand-centred band at 272 nm of the [Nd(F_{20}tpip)$_3$] complex results in the typical lanthanide-centred emission of the trivalent neodymium ion, showing three distinct peaks, corresponding to the $^4F_{3/2}\rightarrow{}^4I_{9/2}$ transition at 875 nm, the $^4F_{3/2}\rightarrow{}^4I_{11/2}$ transition at 1055 nm and the $^4F_{3/2}\rightarrow{}^4I_{13/2}$ transition at 1325 nm (Figure 8). The dominant band in this spectrum is the well-

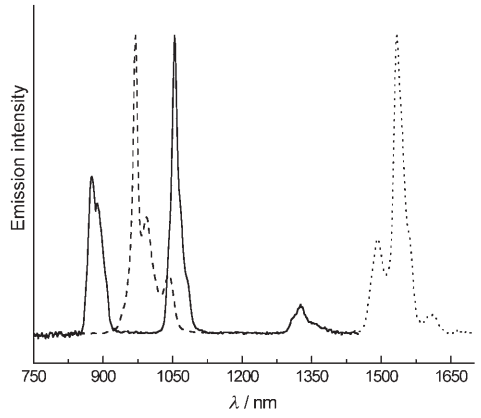

Figure 8. Corrected emission spectrum of [Nd(F_{20}tpip)$_3$] (solid line), [Er(F_{20}tpip)$_3$] (dotted line) and [Yb(F_{20}tpip)$_3$] (dashed line) in dry acetonitrile, $\lambda_{exc}=272$ nm. Emission intensities are not to scale.

known $^4F_{3/2}\rightarrow{}^4I_{11/2}$ transition used in Nd/YAG laser applications. The emission spectrum of the [Er(F_{20}tpip)$_3$] complex (Figure 8, dotted line) shows that the same sensitisation process as discussed for the [Nd(F_{20}tpip)$_3$] complex is valid for [Er(F_{20}tpip)$_3$]. The [Er(F_{20}tpip)$_3$] complex shows the typical $^4I_{13/2}\rightarrow{}^4I_{15/2}$ transition at 1535 nm with some fine structure. The emission spectrum of the [Yb(F_{20}tpip)$_3$] complex in dry acetonitrile (Figure 8) contains one band corresponding to the $^2F_{5/2}\rightarrow{}^2F_{7/2}$ transition. This band is split into three components, the strongest of which is centred at 970 nm, but two weaker components can also be observed, one at 994 nm and another one at 1042 nm.

The excitation spectra of all complexes were recorded by monitoring the strongest emission band in each case. The excitation spectra of all three complexes show a band with $\lambda_{max}=272$ nm, in agreement with the absorption spectra corresponding to the ligand π–π^* absorption band. The spectra of [Eu(F_{20}tpip)$_3$] (Figure 9), [Er(F_{20}tpip)$_3$], [Yb(F_{20}tpip)$_3$]

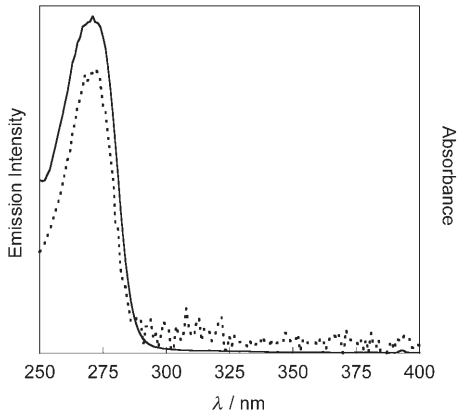

Figure 9. Excitation (solid line) and absorption (dotted line) spectra of [Eu(F_{20}tpip)$_3$] in acetonitrile, $\lambda_{em}=610$ nm.

and [Nd(F_{20}tpip)$_3$] (Supporting Information) are presented. These results demonstrate that energy transfer takes place from the pentafluorophenyl groups of the ligand to the lanthanide ion and that it is the dominant sensitisation pathway for the visible and NIR emitting lanthanides.

The lanthanide emission quantum yields were found to be 0.1% for [Eu(F_{20}tpip)$_3$], [Tb(F_{20}tpip)$_3$] and [Dy(F_{20}tpip)$_3$], and in the [Sm(F_{20}tpip)$_3$] case the signal was too small to calculate a value. The signals were weak compared to the reference compounds and this may attribute to big error values in the measurements. The ligand-based emission of isoabsorptive solutions of [Eu(F_{20}tpip)$_3$] and HF_{20}tpip in acetonitrile was monitored upon excitation at 270 nm. A decrease of ligand emission in [Eu(F_{20}tpip)$_3$] of around 40% indicates that the energy is transferred from the ligand to the Eu^{III} centre. However, the low quantum yields for [Eu(F_{20}tpip)$_3$] and [Tb(F_{20}tpip)$_3$] in comparison with the respective of the tpip complexes[30] (1.3% and 19% for [Eu(tpip)$_3$] and [Tb(tpip)$_3$]) can only be attributed to either additional deactivation processes in the case of F_{20}tpip complexes or to a change of the triplet state level of the ligand. We have excluded the possibility of the presence of other ligand-to-metal charge-transfer states that may provide deactivating pathways due to the lack of any additional bands in the UV/Vis absorption spectra and the fact that both Eu and Tb with different redox properties seemed to be affected. We have also excluded excimer formation based on dilution and solvent effects. To determine the triplet state of F_{20}tpip, we examined the 77 K emission spectrum of the [Gd(F_{20}tpip)$_3$] complex (Figure 10). To our surprise, two bands were observed at 375 and 715 nm. These bands are also present at the room-temperature emission of the [Gd(F_{20}tpip)$_3$] and H(F_{20}tpip); however, in the spectrum of the latter the bands are slightly blue shifted (at 360 and 700 nm) with the low-

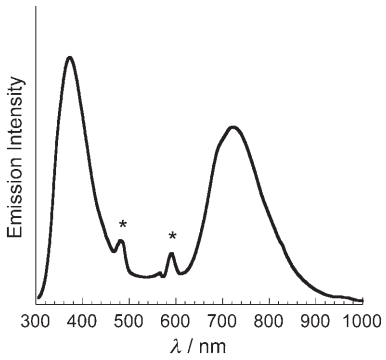

Figure 10. The emission spectrum of $[Gd(F_{20}tpip)_3]$ at 77 K, in MeOH/EtOH 20:80, $\lambda_{exc}=270$ nm. * = scattered light.

energy band being much smaller in intensity relative to the high-energy band (Supporting Information). These results would support the presence of a low-lying ligand-based state which is responsible for an intraligand process that affects the sensitisation of the visible lanthanide emission. The high-energy band can be attributed to the singlet state of the ligand, in agreement with previous reports on photophysical properties of fluorinated benzenes.[51] It is worth noting that DFT calculations support an additional singlet state for pentafluorobenzene with $\pi\sigma^*$ character, lying lower in energy than the $\pi\pi^*$ state.[51] In chloro- and bromobenzenes, dual phosphorescence has been observed at 400 and 500 nm assigned to the $\pi\pi^*$ and $\pi\sigma^*$ states, respectively.[52] The triplet state of fluorobenzenes is less well explored due to the weak signal of emission and reports are limited on studies of single-substituted fluorobenzene.[53,54] Based on our results and the aforementioned reports we attribute the low-energy ligand emission to a π-σ^* state.

Time-resolved luminescence studies of visible and NIR emitting $[Ln(F_{20}tpip)_3]$: The luminescent lifetimes of $[Eu(F_{20}tpip)_3]$, $[Tb(F_{20}tpip)_3]$ and $[Dy(F_{20}tpip)_3]$ have been measured in a variety of solvents, and are presented along with their corresponding radiative rate constants in Table 3. All

Table 3. Luminescence lifetimes in ms at room temperature of the Eu^{III} ($^5D_0$), Tb^{III} ($^5D_4$), and Dy^{III} ($^4F_{9/2}$) levels in $[Ln(F_{20}tpip)_3]$, (Ln = Eu, Tb, Dy), and $\lambda_{exc}=355$ nm.

	Acetonitrile	$[D_3]$Acetonitrile	Acetone	$[D_6]$Acetone
$[Eu(F_{20}tpip)_3]$	1.5	1.6	1.2	3.0
$[Tb(F_{20}tpip)_3]$	1.8	2.0	1.9	1.9
$[Dy(F_{20}tpip)_3]$	0.3	0.3	0.09	0.3

lifetime traces can be fitted satisfactorily to a monoexponential decay profile. The lifetime of the Sm^{III} complex could not be obtained accurately due to the weakness of the signal.

It is evident from these results that solvent coordination affects the lifetime of the complexes. In the cases in which the solvent molecules coordinate strongly with the lanthanide, the effect of deuteration is much more pronounced due to the replacement of C–H bond oscillators with C–D oscillators. The difference in lifetime between acetone and $[D_6]$acetone coordination is more pronounced; the lifetime is more than doubled for the $[Eu(F_{20}tpip)_3]$ complex, and increased by a factor of over three for $[Dy(F_{20}tpip)_3]$. An additional contributing factor is the higher number of C–H vibrations in acetone than acetonitrile in close proximity to the lanthanide centre. This is supported by the close proximity of solvent molecules in the crystal structure of $[Eu(F_{20}tpip)_3]$. Although the crystal structure for $[Dy(F_{20}tpip)_3]$ does not include coordinated solvent molecules, there is enough openness in the structure for coordination in solution. It is also likely that the presence of C–H solvent bonds in the outer coordination sphere of $[Dy(F_{20}tpip)_3]$ will have a slightly larger quenching effect on the luminescence lifetime because of the smaller energy gap ($\approx$7,900 cm^{-1}),[55] between the lowest excited state ($^4F_{9/2}$), and highest J ground state ($^6F_{3/2}$), of the Dy^{III}(aq) ion. The trend is not followed for $[Tb(F_{20}tpip)_3]$, in which only a small increase in lifetime in going from acetone to $[D_6]$acetone is observed. To calculate the number of coordinated solvent molecules[56] we examined the effect of the luminescence lifetimes of upon addition of H_2O and D_2O aliquots (Table 4).

Table 4. Luminescence lifetimes of the Eu^{III} $^5D_0$ level in $[Eu(F_{20}tpip)_3]$ and the Tb^{III} $^5D_4$ level in $[Tb(F_{20}tpip)_3]$ measured at room temperature, $\lambda_{exc}=355$ nm.

	Solvent	τ [ms]
$[Eu(F_{20}tpip)_3]$	dry CH_3CN	1.5
$[Eu(F_{20}tpip)_3]$	dry CH_3CN + H_2O[a]	0.6
$[Eu(F_{20}tpip)_3]$	dry CH_3CN + D_2O[a]	1.5
$[Tb(F_{20}tpip)_3]$	dry CH_3CN	1.8
$[Tb(F_{20}tpip)_3]$	dry CH_3CN + H_2O[a]	0.9
$[Tb(F_{20}tpip)_3]$	dry CH_3CN + D_2O[a]	1.9

[a] $[H_2O]$ and $[D_2O]=10$ mol dm^{-3}.

The application of Equation (1) to the lifetime values (Table 4), in which q = number of coordinated solvent molecules, A is a proportionality constant ($A_{Eu}=1.05$, $A_{Tb}=4.2$), kH_2O is the observed decay rate (ms^{-1}) in an aqueous CH_3CN solution, and k_{CH_3CN} is the observed decay rate (ms^{-1}) in dry CH_3CN, gives values for $[Eu(F_{20}tpip)_3]$ and $[Tb(F_{20}tpip)_3]$ of $q=1.1$ and 2.3, respectively.

$$q = A(k_{H_2O} - k_{CH_3CN}) \quad (1)$$

A modified version of Equation (1) has been proposed[57] taking into account the quenching contribution by outer sphere solvent molecules. The calculated values for $[Eu(F_{20}tpip)_3]$ and $[Tb(F_{20}tpip)_3]$ are $q=0.9$ and 2.4, respectively, by using this method. Based on these q values, there is probably one H_2O molecule coordinated to $[Eu(F_{20}tpip)_3]$ and two H_2O molecules coordinated to $[Tb(F_{20}tpip)_3]$. The reason for the slight increase in hydration states compared with the $[Eu(tpip)_3]$ and $[Tb(tpip)_3]$ complexes may be the result of a greater degree of solvation induced by the polar

C–F bonds. The fluorination of the shell was designed to eliminate all high-energy C–H bonds in the resultant complexes, which would otherwise operate to deactivate f–f-based lanthanide luminescence. Indeed the effect is more pronounced in the case of NIR-emitting complexes.

Powders and solutions of $[Nd(F_{20}tpip)_3]$, $[Er(F_{20}tpip)_3]$ and $[Yb(F_{20}tpip)_3]$ display long luminescence lifetimes (Table 5). All decay curves were monoexponential with good fittings, which confirms the presence of a single species. Deuterated acetonitrile was chosen to provide a C–H vibration-free environment around the lanthanide.

Table 5. Luminescence lifetimes τ in μs of the Nd^{III} ($^4F_{3/2}$), Er^{III} ($^4I_{13/2}$), and Yb^{III} ($^2F_{5/2}$) levels in $[Ln(F_{20}tpip)_3]$, (Ln = Nd, Er, Yb).[a]

	$[Nd(F_{20}tpip)_3]$	$[Er(F_{20}tpip)_3]$	$[Yb(F_{20}tpip)_3]$
powder	46	316	582
solution	44	741	1111

[a] All lifetimes are measured at room temperature, $\lambda_{exc} = 266$ nm, $c = 10^{-5}$ M. All samples were prepared under nitrogen atmosphere. CD_3CN was used as the solvent.

The observed NIR lifetimes represent a substantial and unprecedented increase for Nd, Er or Yb coordination compounds in solution and solid state. The highest value is observed for the $[Yb(F_{20}tpip)_3]$ complex and is more than half the value of the radiative lifetime.[58] The increase in the luminescence decay rate from solution to powder samples, apparent for Er and Yb cases, is in agreement with our previous results in the case of tpip complexes.[29] We have attributed this to crystal lattice vibration or cross relaxation mechanisms operational in solid state. The steep increase in lifetimes from the tpip[29] to the F_{20}tpip shells, indicates that the C–H vibrations in close proximity to the primary and secondary sphere dramatically quench the NIR emission; hence, replacement by C–F is favourable for the emission properties. The solution quantum yields for NIR-emitting complexes can be estimated from $\Phi = \tau/\tau_R$ to be 18% for Nd, 5% for Er and 56% for Yb, in which $\tau_R = 0.25$ ms (Nd^{III}), 14 ms (Er^{III}) and 2 ms (Yb^{III}).

The fluorinated imidodiphosphinate shell is effective for protection of the lanthanide and has been shown to lead to longer lifetimes of the NIR lanthanides than other deuterated or fluorinated ligands.

In summary, it is clear that the effect of the vibrational oscillations (aromatic C–F vs C-H) is different for each case of a visible or NIR emitting lanthanide complex. The ability of bond oscillations to efficiently quench f–f transitions depends primarily upon how closely the emissive states of the lanthanide and the highest energy-level state of the bond oscillators are matched. The ΔE values for the Eu^{III} and Tb^{III} are relatively large, 12300 and ≈ 14800 cm^{-1} respectively; hence, only high-energy vibrational states of (solvent or ligand) bond oscillators will match well and therefore be able to quench the lanthanide excited state effectively. For this reason the effect in the lifetimes is not pronounced in replacing C–H vibrations in tpip with C–F in F_{20}tpip Eu and Tb complexes. Conversely, the energy difference values for a group of lanthanides, which includes Nd^{III} ($\Delta E \approx 5500$ cm^{-1}), Sm^{III} ($\Delta E \approx 7400$ cm^{-1}), Dy^{III} ($\Delta E \approx 7900$ cm^{-1}), Er^{III} ($\Delta E \approx 6500$ cm^{-1}) and Yb^{III} ($\Delta E \approx 10000$ cm^{-1}), are considerably smaller. For these lanthanides it is possible that low-energy vibrational states of bond oscillators quench effectively the excited states. This is supported by our results in which the enhancement of luminescence lifetimes is so pronounced for $[Dy(F_{20}tpip)_3]$ and the NIR-emitting complexes $[Nd(F_{20}tpip)_3]$, $[Er(F_{20}tpip)_3]$ and $[Yb(F_{20}tpip)_3]$, in contrast with the respective tpip complexes.

Conclusions

We have demonstrated that aromatic C–F substitution in an imidodiphosphinate binding site leads to complexes with unparalleled photophysical behaviour in the NIR and visible region. The HF_{20}tpip ligand provides a ligand framework structure that leads to stable, luminescent $[Ln(F_{20}tpip)_3]$ complexes for all lanthanides and provides a ligand framework, with no high-energy X–H vibrations and aryl sensitiser groups, that is able to assemble in a shell arrangement around the metal. The single-crystal structures of the complexes show intermolecular F–F interactions that may lead to the design of new materials and exploration of new applications. The fluorinated shell formed about the lanthanide ion is shown to allow solvent access on the lanthanide coordination sphere, possibly due to the increased polarity of the shell, in contrast with the non-fluorinated, hydrophobic tpip complexes. All of the visible- and NIR-emitting complexes show luminescence that is sensitised by the ligand π–π* state, demonstrated by excitation spectroscopy. The HF_{20}tpip possesses a low-lying π–σ* energy state that affects its sensitiser properties, in particular in the case of the visible emitting complexes $[Ln(F_{20}tpip)_3]$ Ln = Eu, Tb, Sm and Dy. This effect is attributed to the multiple aromatic C–F

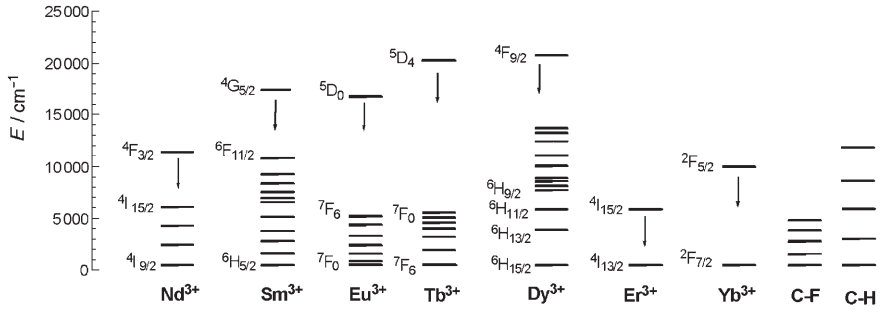

Scheme 3. Representation of the vibrational energy quanta of C–H and C–F bonds and the Ln^{III} low-lying energy electronic levels.

substitution and has not been previously observed in visible-emitting lanthanide complexes of fluorinated diketones. The emission properties of the Dy complex are enhanced to a greater extent in comparison with the rests of the visible lanthanides by C–F substitution. The ligand framework is shown to be ideal for the NIR-emitting lanthanides. The NIR-emitting complexes [Ln(F_{20}tpip)$_3$] with Ln = Nd, Yb and Er show unprecedented long lifetimes that will undoubtedly lead to exciting application of NIR complexes in imaging applications and luminescent materials. The [Yb(F_{20}tpip)$_3$] complex shows a luminescence lifetime more than half the value of the radiative ion lifetime. The results show that the elimination of high-energy X–H vibrations in the ligand structure and elimination of solvent coordination are two factors particularly important for the yellow emission of Dy and the NIR emission of Nd, Yb and Er lanthanides.

Experimental Section

Equipment: ^{1}H, ^{13}C, ^{19}F{^{1}H} and ^{31}P{^{1}H} NMR spectra were recorded on Bruker AC300, AV300, AV400 and DRX 500 spectrometers. Orthophosphoric acid was used as an external reference for ^{31}P{^{1}H} shifts, and CCl_3F was as the external reference for ^{19}F shifts. Elemental analyses were performed by the CHN microanalysis services at University of London. Fast atom bombardment mass spectra (FAB MS) were measured on a VG ZabSpec machine by using a Cs neutral atom beam. Electrospray mass spectra were recorded on a Micromass LC-TOF machine. UV/Vis absorption spectra were recorded on a Shimadzu UV-3101PC UV/Vis/NIR and Perkin–Elmer Lambda 17 spectrometers. All measurements were carried out at room temperature (≈20 °C) unless otherwise stated. Luminescence experiments of the visible-emitting lanthanide complexes were carried out on a Photon Technology Instruments emission spectrometer previously described.[59] Emission spectra were corrected for the PMT response. Excitation spectra were corrected for lamp response. Lifetime spectra were carried out by using a Photon Technology Instruments system equipped with Continuum Surelite SSP Nd-YAG laser, using the 355 nm harmonic excitation light.[30] The data for the lifetime studies were recorded on a LeCroy 9350 AM 500 MHz oscilloscope, as an average of 500 shots and analysed using a non-linear least-squares iterative technique (Marquardt–Levenberg algorithm).

The steady-state luminescence spectra and the lifetime measurements in the NIR were done on an Edinburgh Instruments FS920P near-infrared spectrometer, with a 450W xenon lamp as the steady-state excitation source, a double excitation monochromator with 1800 lines per mm, an emission monochromator with 600 lines per mm and a liquid nitrogen cooled Hamamatsu R5509–72 near infrared photomultiplier tube. For the lifetime measurements, the setup includes a Nd/YAG laser, equipped with 2nd, 3rd and 4th harmonic options (allowing laser excitation at 532, 355 and 266 nm, respectively). Repetition rate is 10 Hz, pulse width is 3–5 ns. A maximum value of an error of 15% is estimated for all lifetime measurements.

For the determination of X-ray crystal structures, intensity data were collected on Brüker SMART 6000 diffractometers equipped with CCD detectors using $Cu_{K\alpha}$ radiation $\lambda = 1.54178$ Å). The images were interpreted and integrated with the program SAINT.[60] SHELX97 was used for solution and refinement.[61] The structures were solved by direct methods and refined by full-matrix least-squares methods on F^2. Non-hydrogen atoms were refined anisotropically and the riding mode was used for hydrogen atoms. CCDC-634236–634244 contain the supplementary crystallographic data for this paper. These data can be obtained free of charge from The Cambridge Crystallographic Data Centre via www.ccdc.cam.ac.uk/data_request/cif.

Materials: Starting materials were of reagent grade, obtained from Aldrich or Avocado, and used without further purification, unless otherwise stated. Bromopentafluorobenzene (98%) was obtained from Avocado and dried with 4 Å molecular sieves prior to use. Lanthanide(III) chlorides were obtained from Aldrich or Acros (99.9%) and used as received. Deuterated solvents were obtained from Goss Scientific and used as received. Anhydrous solvents, when required, were freshly distilled over the appropriate drying agents under dinitrogen. Reactions requiring anhydrous conditions were performed under dinitrogen using standard Schlenk and vacuum line techniques. For the photophysical studies CH_3CN was dried over P_2O_5 (5% w/v) and freshly distilled prior to use, [D_6]acetone, [D_3]acetonitrile and acetone used in photophysical studies were dried over 3 Å molecular sieves.

Bromodipentafluorophenylphosphane: The preparation was carried out in a N_2 atmosphere in dry conditions. A solution of bromopentafluorobenzene (10.0 g, 5.05 mL, 40.5 mmol) in dry diethyl ether was added dropwise to a suspension of Mg turnings (1.07 g, 44.0 mmol) in dry diethyl ether (10 mL), at a rate to keep the solution under a gentle reflux. A small crystal of iodine was used to initiate the reaction. The solution was then heated under reflux for 2 h. The resulting dark brown solution was transferred slowly through a canula to a solution of phosphorus tribromide (1.7 mL, 4.7 g, 18.0 mmol) in dry diethyl ether (6 mL) on a salt-ice bath. The solution was stirred for 1 h, after which anhydrous benzene (30 mL) was added. The diethyl ether was removed under reduced pressure giving a large amount of precipitate. The solution was filtered under N_2 and the benzene removed at reduced pressure giving a thick brown liquid. The crude product was purified by distillation at 0.1 Torr with the desired fraction coming over at 100–104 °C to yield the desired product as a thick golden oil (4.35 g, 9.8 mmol, 54%). ^{31}P{^{1}H} NMR (121 MHz, $CDCl_3$): $\delta = 12.8$ ppm (quint, ^3J (P,F) = 36 Hz); ^{19}F{^{1}H} NMR (282 MHz, $CDCl_3$): $\delta = -127.9$ (m, 4F; *o*-Ar CF), −146.2 (tt, ^3J(F,F) = 20 Hz, ^4J(F,F) = 4 Hz, 2F; *p*-Ar CF), −159.1 ppm (m, 4F; *m*-Ar CF). In a previous publication the only spectroscopic analysis reported is ^{31}P NMR spectrum, which agrees with our result.[44,62] Mass spectrometry was not attempted due to the air and moisture sensitivity of the compound.

***N*-(*P,P*-Dipentafluorophinoyl)-*P,P*-dipentafluorophenylphosphinimidic acid (HF_{20}tpip)**: Hexamethyldisilazane (0.82 mL, 0.63 g, 3.9 mmol) was added to a solution of bromodipentafluorophenylphosphane (5.14 g, 11.6 mmol) in toluene (20 mL). The solution was heated under reflux for 5 h then the byproduct Me_3SiBr removed by distillation. The resulting brown solution was cooled on an ice bath for 10 min and hydrogen peroxide (1.1 g, 11.6 mmol, 35% in water) in THF (9 mL) was slowly added dropwise. The contents of the flask were added to diethyl ether (100 mL). The solution was filtered and the solvent removed. The crude product was separated on silica 90 using hexane/ethyl acetate/acetic acid (50:50:1) to give the product as a pale cream solid (0.98 g, 1.3 mmol, 33%). HF_{20}tpip crystals were grown by slow evaporation of the chromatography solutions. ^{31}P{^{1}H} NMR (121 MHz, [D_6]acetone): $\delta = -9.0$ ppm (s); ^{19}F{^{1}H} NMR (282 MHz, [D_6]acetone): $\delta = -134.8$ (d, ^3J(F,F) = 21 Hz, 8F; *o*-Ar CF), −148.9 (t, ^3J(F,F) = 20 Hz, 4F; *p*-Ar CF), −162.8 ppm (br, ^3J(F,F) = 21 Hz, 8F; *m*-Ar CF); ^{13}C NMR (75 MHz, [D_6]acetone): $\delta = 149$ (d, ^1J(C,F) = 250 Hz, 8C; Ar CF), 145 (d, ^1J(C,F) = 260 Hz, 4C; Ar CF), 139 (d, ^1J(C,F) = 250 Hz, 8C; Ar CF), 114 ppm (dt, ^1J (C,P) = 140 Hz, ^2J(C,F) = 18 Hz, 4C; C_{quat}); accurate MS (ESI$^+$): *m/z*: calcd for [M^+ +Na]: 799.9061; found: 799.9066; UV/Vis (ethanol): λ_{max} (log ε) = 268 nm (3.6); elemental analysis calcd (%) for $C_{24}F_{20}NO_2P_2H{\cdot}1.5\,H_2O$: C 35.8, H 0.5, N 1.7; found: C 35.9, H 0.5, N 1.7.

Crystallographic data: $C_{24}HF_{20}NO_2P_2{\cdot}0.25(C_6H_{14})$, $M_r = 798.74$, orthorhombic, space group *Pbcn*, $a = 12.3361(4)$, $b = 22.0894(6)$, $c = 21.9459(6)$ Å, $V = 5980.2(3)$ Å^3, $Z = 8$, $\rho_{calcd} = 1.774$ g cm^{-3}, $F(000) = 3124$, $\mu = 2.782$ mm^{-1}, $R1 = 0.0512$ [$2\sigma F$], $wR = 0.148$ for 4142 independent reflections.

[Ln(F_{20}tpip)$_3$] with Ln = Y, Nd, Sm, Eu, Gd, Tb, Dy, Er, Yb: $LnCl_3{\cdot}x\,H_2O$ (0.017 mmol, 1 equiv) in ethanol (2 mL) followed by a solution of potassium hydroxide in methanol (0.17 mL, 0.017 mmol, 0.1 M) were added to a stirring solution of HF_{20}tpip (40 mg, 0.052 mmol, 3 equiv) in hot ethanol. The solution was heated under reflux for 1 h and allowed to cool to room temperature. The resulting white precipitate was collected by filtration,

washed with methanol, and then dried under vacuum to give the corresponding [Ln(F_{20}tpip)$_3$]. Typical yields 60–95%. Single crystals for X-ray diffraction and solid-state luminescence studies were grown from solutions of the complex in methanol with 10% acetone. The same preparation without the addition of bases was successfully attempted where Ln = Y, Eu, Tb, Dy.

[Y(F_{20}tpip)$_3$]: $^{31}P\{^1H\}$ NMR (121 MHz, [D$_6$]acetone): $\delta = -3.2$ ppm (s); $^{19}F\{^1H\}$ NMR (282 MHz, [D$_6$]acetone): $\delta = -133.6$ (d, $J = 20$ Hz, 8F; *o*-Ar CF), −148.3 (t, $J = 19$ Hz, 4F; *p*-Ar CF), −162.1 ppm (t, $J = 20$ Hz, 8F; *m*-Ar CF); MS (FAB$^+$): *m*/*z*: 2417 [M^++H], 1640 [$M^+ - C_{24}F_{20}NP_2O_2$].

[Nd(F_{20}tpip)$_3$]: $^{31}P\{^1H\}$ NMR (121 MHz, [D$_6$]acetone): $\delta = 7.4$ ppm (s); $^{19}F\{^1H\}$ NMR (282 MHz, [D$_6$]acetone): $\delta = -133.7$ (d, $J = 19$ Hz, 8F; *o*-Ar CF), −149.0 (t, $J = 20$ Hz, 4F; *p*-Ar CF), −162.3 ppm (m, 8F; *m*-Ar CF); MS (ES$^+$): *m*/*z*: 2496 [M^++Na]; UV/Vis (acetonitrile): λ_{max} ($\log\varepsilon$) = 272 nm (4.1); elemental analysis calcd (%) for $C_{72}F_{60}N_3NdO_6P_6$: C 35.0, H 0.0, N 1.7; found: C 34.9, H 0.0, N 1.9.

[Sm(F_{20}tpip)$_3$]: $^{31}P\{^1H\}$ NMR (121 MHz, [D$_6$]acetone): $\delta = -3.7$ ppm (s); $^{19}F\{^1H\}$ NMR (282 MHz, [D$_6$]acetone): $\delta = -133.5$ (d, ^3J(F,F) = 19 Hz, 8F; *o*-Ar CF), −148.8 (t, ^3J(F,F) = 20 Hz, 4F; *p*-Ar CF), −162.2 ppm (m, 8F; *m*-Ar CF); ^{13}C NMR (75 MHz, [D$_6$]acetone): $\delta = 149$ (d, ^1J(C,F) = 257 Hz; Ar CF), 146 (d, ^1J(C,F) = 264 Hz; Ar CF), 139 (d, ^1J(C,F) = 252 Hz; Ar CF), 112 ppm (dt, ^1J (C,P) = 144 Hz, ^2J(C,F) = 18 HzM; Ar C); MS (FAB$^+$): *m*/*z*: 2480 [M^++H], 1704 [$M^+ - C_{24}F_{20}NP_2O_2$]; UV/Vis (acetonitrile): λ_{max} ($\log\varepsilon$) = 272 nm (4.1); elemental analysis calcd (%) for $C_{72}F_{60}N_3O_6P_6Sm$: C 34.9, H 0.0, N 1.7; found: C 35.0, H 0.0, N 1.7.

[Eu(F_{20}tpip)$_3$]: $^{31}P\{^1H\}$ NMR (121 MHz, [D$_6$]acetone): $\delta = -39.4$ ppm (s); $^{19}F\{^1H\}$ NMR (282 MHz, [D$_6$]acetone): $\delta = -132.9$ (d, ^3J(F,F) = 20 Hz, 8F; *o*-Ar CF), −148.8 (t, ^3J(F,F) = 20 Hz, 4F; *p*-Ar CF), −162.2 ppm (m, 8F; *m*-Ar CF); MS (ESI$^+$): *m*/*z*: 2496 [M^++Na]; UV/Vis (acetonitrile): λ_{max} ($\log\varepsilon$) = 272 nm (4.2); elemental analysis calcd (%) for $C_{72}EuF_{60}N_3O_6P_6$: C 34.9, H 0.0, N 1.7; found: C 35.1, H 0.0, N 1.8.

[Gd(F_{20}tpip)$_3$]: MS (FAB$^+$): *m*/*z*: 2509 [M^++Na], 2487 [M^++H], 1710 [$M^+ - C_{24}F_{20}NP_2O_2$]; UV/Vis (acetonitrile): λ_{max} ($\log\varepsilon$) = 272 nm (4.1); elemental analysis calcd (%) for $C_{72}F_{60}GdN_3O_6P_6$: C 34.8, H 0.0, N 1.7; found: C 34.8, H 0.0, N 1.9.

[Tb(F_{20}tpip)$_3$]: $^{31}P\{^1H\}$ NMR (121 MHz, [D$_6$]acetone): $\delta = -11.5$ ppm (brs); $^{19}F\{^1H\}$ NMR (282 MHz, [D$_6$]acetone): $\delta = -131.8$ (br, 8F; *o*-Ar CF), −149.2 (br, 4F; *p*-Ar CF), −162.9 ppm (br, 8F; *m*-Ar CF); MS (ESI$^+$): *m*/*z*: 2511 [M^++Na]; UV/Vis (acetonitrile): λ_{max} ($\log\varepsilon$) = 272 nm (4.1); elemental analysis calcd (%) for $C_{72}F_{60}N_3O_6P_6Tb$: C 34.8, H 0.0, N 1.7; found: C 35.0, H 0.0, N 1.7.

[Dy(F_{20}tpip)$_3$]: $^{31}P\{^1H\}$ NMR (121 MHz, [D$_6$]acetone): $\delta = -3.1$ ppm (brs); $^{19}F\{^1H\}$ NMR (282 MHz, [D$_6$]acetone): $\delta = -129.7$ (br, 8F; *o*-Ar CF), −149.0 (br, 4F; *p*-Ar CF), −162.5 ppm (br, 8F; *m*-Ar CF); MS (FAB$^+$): *m*/*z*: 2493 [M^++H], 1716 [$M^+ - C_{24}F_{20}NP_2O_2$]; UV/Vis (acetonitrile): λ_{max} ($\log\varepsilon$) = 272 nm (3.9); elemental analysis calcd (%) for $C_{72}DyF_{60}NO_6P_6$: C 34.7, H 0.0, N 1.7; found: C 34.8, H 0.0, N 1.8.

[Er(F_{20}tpip)$_3$]: $^{31}P\{^1H\}$ NMR (121 MHz, [D$_6$]acetone): $\delta = -46.6$ ppm (brs); $^{19}F\{^1H\}$ NMR (282 MHz, [D$_6$]acetone): $\delta = -133.0$ (br, 8F; *o*-Ar CF), −148.0 (br, 4F; *p*-Ar CF), −161.9 ppm (br, 8F; *m*-Ar CF); MS (FAB$^+$): *m*/*z* 2497 [M^++H], 1720 [$M^+ - C_{24}F_{20}NP_2O_2$]; UV/Vis (acetonitrile): λ_{max} ($\log\varepsilon$) = 272 nm (4.1); elemental analysis calcd (%) for $C_{72}ErF_{60}NO_6P_6$: C 34.6, H 0.0, N 1.7; found: C 34.7, H 0.0, N 1.6.

[Yb(F_{20}tpip)$_3$]: $^{31}P\{^1H\}$ NMR (121 MHz, [D$_6$]acetone): $\delta = -0.26$ ppm (brs); $^{19}F\{^1H\}$ NMR (282 MHz, [D$_6$]acetone): $\delta = -134.6$ (br, 8F; *o*-Ar CF), −147.5 (br, 4F; *p*-Ar CF), −161.9 ppm (br, 8F; *m*-Ar CF); MS (FAB$^+$): *m*/*z* 2502 [M^+]; UV/Vis (acetonitrile): λ_{max} ($\log\varepsilon$) = 272 nm (4.1); elemental analysis calcd (%) for $C_{72}F_{60}NO_6P_6Yb$: C 34.5, H 0.0, N 1.7; found: C 34.6, H 0.0, N 1.9.

Acknowledgement

We wish to thank EPSRC and the University of Birmingham for support. R.V.D. is a postdoctoral fellow of the FWO-Flanders and he gratefully acknowledges a Research Grant of the Fund for Scientific Research—Flanders (FWO; project 1.5.099.06).

[1] K. Zeckert, J. Hamacek, J. M. Senegas, N. Dalla-Favera, S. Floquet, G. Bernardinelli, C. Piguet, *Angew. Chem.* **2005**, *117*, 8168; *Angew. Chem. Int. Ed.* **2005**, *44*, 7954.
[2] S. Floquet, M. Borkovec, G. Bernardinelli, A. Pinto, L. A. Leuthold, G. Hopfgartner, D. Imbert, J. C. G. Bünzli, C. Piguet, *Chem. Eur. J.* **2004**, *10*, 1091.
[3] N. Andre, R. Scopelliti, G. Hopfgartner, C. Piguet, J. C. G. Bünzli, *Chem. Commun.* **2002**, 214.
[4] A. P. Bassett, S. W. Magennis, P. B. Glover, D. J. Lewis, N. Spencer, S. Parsons, R. M. Williams, L. De Cola, Z. Pikramenou, *J. Am. Chem. Soc.* **2004**, *126*, 9413.
[5] O. Mamula, M. Lama, S. G. Telfer, A. Nakamura, R. Kuroda, H. Stoeckli-Evans, R. Scopelitti, *Angew. Chem.* **2005**, *117*, 2583; *Angew. Chem. Int. Ed.* **2005**, *44*, 2527.
[6] M. T. Gamer, P. W. Roesky, *Inorg. Chem.* **2005**, *44*, 5963.
[7] Y. Bretonniere, M. Mazzanti, J. Pecaut, M. M. Olmstead, *J. Am. Chem. Soc.* **2002**, *124*, 9012.
[8] Y. J. Zhang, B. Q. Ma, S. Gao, J. R. Li, Q. D. Liu, G. H. Wen, X. X. Zhang, *J. Chem. Soc. Dalton Trans.* **2000**, 2249.
[9] J. B. Livramento, A. Sour, A. Borel, A. E. Merbach, V. Toth, *Chem. Eur. J.* **2006**, *12*, 989.
[10] P. B. Glover, P. R. Ashton, L. J. Childs, A. Rodger, M. Kercher, R. M. Williams, L. De Cola, Z. Pikramenou, *J. Am. Chem. Soc.* **2003**, *125*, 9918.
[11] M. M. Castaño-Briones, A. P. Bassett, L. L. Meason, P. R. Ashton, Z. Pikramenou, *Chem. Commun.* **2004**, 2832.
[12] S. W. Magennis, J. Craig, A. Gardner, F. Fucassi, P. J. Cragg, N. Robertson, S. Parsons, Z. Pikramenou, *Polyhedron* **2003**, *22*, 745.
[13] D. J. Hoffart, S. J. Loeb, *Angew. Chem.* **2005**, *117*, 923; *Angew. Chem. Int. Ed.* **2005**, *44*, 901.
[14] D. Guo, C.-y. Duan, F. Lu, Y. Hasegawa, Q.-j. Menga, S. Yanagida, *Chem. Commun.* **2004**, 1486.
[15] J. M. Herrera, S. J. A. Pope, H. Adams, S. Faulkner, M. D. Ward, *Inorg. Chem.* **2006**, *45*, 3895.
[16] S. Comby, R. Scopelliti, D. Imbert, L. Charbonniere, R. Ziessel, J. C. G. Bünzli, *Inorg. Chem.* **2006**, *45*, 3158.
[17] Y. F. Zhou, M. Hong, X. T. Wu, *Chem. Commun.* **2006**, 135.
[18] Y. Wan, L. Zhang, L. Jin, S. Gao, S. Lu, *Inorg. Chem.* **2003**, *42*, 4985.
[19] X. P. Yang, R. A. Jones, V. Lynch, M. Oye, A. L. Holmes, *Dalton Trans.* **2005**, 849.
[20] Z. Spichal, M. Necas, J. Pinkas, *Inorg. Chem.* **2005**, *44*, 2074.
[21] V. Patroniak, A. R. Stefankiewicz, J. M. Lehn, M. Kubicki, M. Hoffmann, *Eur. J. Inorg. Chem.* **2006**, 144.
[22] J. C. G. Bünzli, *Acc. Chem. Res.* **2006**, *39*, 53.
[23] P. Coppo, M. Duati, V. N. Kozhevnikov, J. W. Hofstraat, L. De Cola, *Angew. Chem.* **2005**, *117*, 1840; *Angew. Chem. Int. Ed.* **2005**, *44*, 1806.
[24] R. Delgado, J. Costa, K. P. Guerra, L. M. P. Lima, *Pure Appl. Chem.* **2005**, *77*, 569.
[25] D. J. Lewis, T. M. Day, J. V. MacPherson, Z. Pikramenou, *Chem. Commun.* **2006**, 1433.
[26] J. Yang, Q. Yuo, G. D. Li, J. J. Cao, G. H. Li, J. S. Chen, *Inorg. Chem.* **2006**, *45*, 2857.
[27] T. Gunnlaugsson, J. P. Leonard, *Chem. Commun.* **2005**, 3114.
[28] J. H. Yu, D. Parker, R. Pal, R. A. Poole, M. J. Cann, *J. Am. Chem. Soc.* **2006**, *128*, 2294.
[29] A. P. Bassett, R. Van Deun, P. Nockemann, P. B. Glover, B. M. Kariuki, K. Van Hecke, L. Van Meervelt, Z. Pikramenou, *Inorg. Chem.* **2005**, *44*, 6140.
[30] S. W. Magennis, S. Parsons, Z. Pikramenou, *Chem. Eur. J.* **2002**, *8*, 5761.
[31] S. W. Magennis, S. Parsons, A. Corval, J. D. Woollins, Z. Pikramenou, *Chem. Commun.* **1999**, 61.
[32] A.-S. Chauvin, F. Gumy, I. Matsubayashi, Y. Hasegawa, J. C. G. Bünzli, *Eur. J. Inorg. Chem.* **2006**, 473.

[33] S. Yanagida, Y. Hasegawa, K. Murakoshi, Y. Wada, N. Nakashima, T. Yamanaka, *Coord. Chem. Rev.* **1998**, *171*, 461.
[34] Y. Hasegawa, Y. Kimura, K. Murakoshi, Y. Wada, J.-H. Kim, N. Nakashima, T. Yamanaka, S. Yanagida, *J. Phys. Chem.* **1996**, *100*, 10201.
[35] Y. Hasegawa, K. Murakoshi, Y. Wada, S. Yanagida, J.-H. Kim, N. Nakashima, C. Yamanaka, *Chem. Phys. Lett.* **1996**, *248*, 8.
[36] Y. Zheng, J. Lin, Y. Liang, Q. Lin, Y. Yu, Q. Meng, Y. Zhou, S. Wang, H. Wang, H. Zhang, *J. Mater. Chem.* **2001**, *11*, 2615.
[37] H. J. Batista, A. V. M. De Andrade, R. L. Longo, A. M. Simas, G. F. De Sa, N. K. Ito, L. C. Thompson, *Inorg. Chem.* **1998**, *37*, 3542.
[38] N. V. Rusakova, Z. M. Topilova, S. B. Meshkova, M. O. Lozinskii, Y. I. Gevaza, *Russ. J. Inorg. Chem.* **1992**, *37*, 116.
[39] G. A. Hebbink, D. N. Reinhoudt, F. C. J. M. van Veggel, *Eur. J. Org. Chem.* **2001**, 4101.
[40] Y. Hasegawa, T. Ohkubo, K. Sogabe, Y. Kawamura, Y. Wada, N. Nakashima, S. Yanagida, *Angew. Chem.* **2000**, *112*, 365; *Angew. Chem. Int. Ed.* **2000**, *39*, 357.
[41] R. Van Deun, P. Nockemann, C. Görller-Walrand, K. Binnemans, *Chem. Phys. Lett.* **2004**, *397*, 447.
[42] P. B. Glover, PhD thesis, University of Birmingham (UK), **2004**.
[43] G. Mancino, A. Ferguson, A. Beeby, N. J. Long, T. S. Jones, *J. Am. Chem. Soc.* **2005**, *127*, 524.
[44] R. Ali, K. B. Dillon, *J. Chem. Soc. Dalton Trans.* **1990**, 2593.
[45] A. Cairncross, W. A. Sheppard, E. Wonchoba, *Org. Synth.* **1988**, *VI*, 875.
[46] M. Fild, O. Glemser, I. Hollenburg, *Z. Naturforsch. B* **1966**, *21*, 920.
[47] A. M. Trzeciak, H. Bartosz-Bechowski, Z. Ciunik, K. Niesyty, J. J. Ziolkowski, *Can. J. Chem.* **2001**, *79*, 752.
[48] J. A. S. Howell, N. Fey, J. D. Lovatt, P. C. Yates, P. McArdle, D. Cunningham, E. Sadeh, H. E. Gottlieb, Z. Goldschmidt, M. B. Hursthouse, M. E. Light, *J. Chem. Soc. Dalton Trans.* **1999**, 3015.
[49] J. C. G. Bünzli, G. R. Choppin in *Lanthanide Probes in Life, Chemical and Earth Sciences*, Elsevier Science, Amsterdam, **1989**.
[50] R. S. Drago in *Physical Methods for Chemists*, 2nd ed., Saunders, Philadelphia, **1992**.
[51] M. Z. Zgierski, T. Fujiwara, E. C. Lim, *J. Chem. Phys.* **2005**, *122*, 144312.
[52] T. Takemura, Y. Yamada, M. Sugawara, H. Baba, *J. Phys. Chem.* **1986**, *90*, 2324.
[53] T. Okutsu, K. I. H. Haneda, H. Hiratsuka, *Chem. Phys. Lett.* **2002**, *355*, 48.
[54] I. Unger, *J. Phys. Chem.* **1965**, *69*, 4284.
[55] W. T. Carnall, P. R. Fields, K. Rajnak, *J. Chem. Phys.* **1968**, *49*, 4424.
[56] W. D. Horrocks Jr. , D. R. Sudnick, *Acc. Chem. Res.* **1981**, *14*, 384.
[57] A. Beeby, I. M. Clarkson, R. S. Dickins, S. Faulkner, D. Parker, L. Royle, A. S. De Sousa, J. A. G. Williams, M. Woods, *J. Chem. Soc. Perkin Trans. 2* **1999**, 493.
[58] M. H. V. Werts, J. W. Verhoeven, J. W. Hofstraat, *Perkin Trans. 2* **2000**, 433.
[59] J. M. Haider, M. Chavarot, S. Weidner, I. Sadler, R. M. Williams, L. De Cola, Z. Pikramenou, *Inorg. Chem.* **2001**, *40*, 3912.
[60] SAINT (manual version) 5.0/6.0 ed. Bruker Analytical Z-ray Systems (USA), **1997**.
[61] G. M. Sheldrick, SHELX97, University of Gottingen (Germany).
[62] R. Ali, K. B. Dillon, *Polyhedron* **1986**, *5*, 1197.

Received: January 19, 2007
Published online: June 15, 2007

